Fast InSAR Phase Unwrapping Method for Complex Mountainous Areas With High Noise and Large Gradient Changes

Dingyi Zhou and Zhifang Zhao

***Abstract*—Interferometry synthetic aperture radar (InSAR) is essential for monitoring surface deformation and geological hazards. InSAR applications in complex mountainous regions are challenging due to high noise levels and large phase gradient variations, which make it difficult to obtain accurate and efficient phase unwrapping results. As a result, the development of fast and high-precision phase unwrapping methods in these areas has become an urgent research topic in the current InSAR field. In response to this challenge, this study proposes a fast and high-precision phase unwrapping method specifically designed for complex mountainous regions. The method includes a sliding window singular value denoising phase gradient correction unwrapping algorithm (SDPC) for obtaining precise phase unwrapping results. A fast-phase unwrapping algorithm based on FPUNet networks is proposed by integrating deep learning techniques with the SDPC results. By integrating these two methods, the phase unwrapping speed can be accelerated while maintaining the unwrapping accuracy. The Dongchuan District of Kunming City, Yunnan Province, is used as the subject of this article. Because the true phase cannot be known using the measured interferometric phase data, simulated data are introduced to verify and demonstrate the validity and accuracy of the method presented in this article. Experimental results demonstrate the effectiveness of the proposed method for phase unwrapping, even in complex mountainous regions characterized by high noise and large gradient variations. Moreover, this approach significantly enhances the phase unwrapping speed. The presented method addresses the inefficiency and inaccuracy of InSAR in phase unwrapping in complex mountainous regions.**

***Index Terms*—Complex mountainous area, deep learning, high noise, interferometry synthetic aperture radar (InSAR) phase unwrapping, large gradient changes.**

Manuscript received 7 March 2024; revised 6 May 2024 and 12 June 2024; accepted 18 June 2024. Date of publication 24 June 2024; date of current version 8 July 2024. This work was supported in part by the National Natural Science Foundation of China under Grant 42161067, in part by the Postgraduate Research and Innovation Foundation of Yunnan University under Grant KC-23236484, and in part by Yunnan Provincial Department of Education Science Research Fund Project under Grant 2023Y0196. *(Corresponding author: Zhifang Zhao.)*

Dingyi Zhou is with the Institute of International Rivers and Eco-Security, Yunnan University, Kunming 650500, China (e-mail: zhoudingyi@mail.ynu.edu.cn).

Zhifang Zhao is with the Institute of International Rivers and Eco-Security, Yunnan University, Kunming 650500, China, also with the School of Earth Sciences, Yunnan University, Kunming 650500, China, also with the Research Center of Domestic High-resolution Satellite Remote Sensing Geological Engineering, Kunming 650500, China, also with the Yunnan Key Laboratory of Sanjiang Metallogeny and Resources Exploration and Utilization, Kunming 650051, China, also with the Key Laboratory of Sanjiang Metallogeny and Resources Exploration and Utilization, MNR, Kunming 650051, China, and also with the Yunnan International Joint Laboratory of China-Laos-Bangladesh-Myanmar Natural Resources Remote Sensing Monitoring, Kunming 650051, China (e-mail: zhaozhifang@ynu.edu.cn).

Digital Object Identifier 10.1109/JSTARS.2024.3417417

I. Introduction

GIVEN the rising count of SAR satellites, the widespread adoption of interferometric synthetic aperture radar (InSAR) technology has become significant. It serves a vital purpose in monitoring surface deformation, identifying geological disasters, and tracking glacier movements [1], [2], [3]. Unwrapping the phase is an essential step in processing InSAR interferometric data. It effectively reconstructs the authentic phase from the wrapped phase within the range of $(-\pi, \pi]$. This step is crucial for extracting elevation parameters or deformation information [4], [5]. Obtaining accurate and efficient unwrapped phase results in complex mountainous regions is challenging due to high noise and large gradient variations. Therefore, quickly obtaining high-precision phase unwrapping results in these regions has become an urgent challenge in the InSAR field [6], [7].

Numerous phase unwrapping algorithms have emerged and found applications in InSAR data processing. These algorithms can broadly be categorized into three groups. One category includes classical path tracing algorithms, such as the branch-cut (BC) method [8] and the quality-guided method [9]. These algorithms use prior information from the interferogram to select the integration path and then integrate the estimated phase gradient to obtain the unwrapped phase. This approach can effectively prevent local errors from propagating globally and achieve high computational efficiency and accuracy. Another type is represented by global optimality algorithms, such as the minimum norm classes [10], [11] and network flows [4]. The least-squares method is an exemplary algorithm belonging to the minimum-norm class of algorithms. However, the least-squares method often produces excessively curved surfaces when dealing with interferograms with a low signal-to-noise (S/N) ratio. Minimum cost flow (MCF) is currently the most common algorithm used in engineering applications for phase unwrapping. This algorithm achieves the unwrapped phase by obtaining the optimal estimate of the phase gradient, thereby enhancing the precision and efficiency of InSAR phase unwrapping. However, the algorithm's accuracy is difficult to guarantee due to the difficulty in determining the unbiased coherence factor and other weighting factors [12], [13]. The above two kinds of

algorithms can get good results when dealing with high S/N ratio interferograms, but the phase unwrapping results are poor for low S/N interferograms. At the same time, estimating the phase gradient is an essential factor in both algorithms' accuracy of the unwrapping results. Standard gradient estimation methods rely on the assumption of phase continuity, which posits that the wrapped phase gradient can yield the true phase gradient in a noise-free scenario. In addition, the continuity assumption limits the phase gradients between $(-\pi, \pi]$, making it challenging to obtain ideal phase unwrapping results in regions with large gradient variations. The last type is the nonlinear filtering phase unwrapping algorithm represented by the extended Kalman filtering [14]. This algorithm converts the problem of phase unwrapping into an estimation task. The advantage lies in the fact that it enables phase unwrapping and performs noise filtering. However, this requires a longer processing time, making it difficult for this method to obtain phase unwrapping information quickly. In summary, these algorithms still have some limitations in solving the phase unwrapping problem in regions with high noise and large gradient variation, such as vulnerability to noise interference and the requirement of large computational resources. Therefore, further research and development of phase unwrapping algorithms are still necessary. Some scholars use maximum likelihood estimation to accurately estimate phase gradients in noisy interferograms [15]. However, the phase gradient estimation results could be more reliable when the noise is large. At the same time, using the Chinese remainder theorem solves the problem of large gradient variations in multibaseline interferograms. Still, this method cannot be used for single-scene images; thus, its application is limited [16]. Due to its high efficiency in phase unwrapping, the minimum norm algorithm has been the subject of intense research. It is simple in principle, converges fast, and has many applications [17], [18]. Among them, the iterative least-squares method is an effective method to solve the problem of overfitting in low-SNR interferograms. With the gradual integration of deep learning into interferogram-based phase unwrapping [19], [20], [21], [22], it effectively avoids the need for traditional phase unwrapping methods that consume a large number of computing resources and time. Moreover, deep learning can adaptively learn features and hence adapt to different interferogram data and phase unwrapping problems, making it more widely applicable. However, existing deep learning phase unwrapping methods have the following issues. 1) Interferometric phase samples are obtained based on existing phase unwrapping methods. It inevitably makes it unsuitable for regions with high noise and large gradient variations. Therefore, there is a need for a phase unwrapping method suitable for complex mountainous environments as a training set for deep learning. 2) Most experiments were carried out on simulated data and only considered phase unwrapping results in small regions, using 256×256 pixel interferometric simulated phases for the experiments. Less research has been done on the practical applications of deep learning for phase unwrapping using large-scale interferometric phase data in complex mountainous environments.

This article addresses the challenge of obtaining fast InSAR phase unwrapping results in complex mountainous regions with high noise and large gradient variation. First, a phase gradient corrected phase unwrapping algorithm based on iterative least squares (ILSs) with sliding window singular value decomposition is proposed to obtain accurate phase gradient results in these regions. Second, using this phase unwrapping algorithm, we present a rapid phase unwrapping algorithm utilizing the FPUNet network, which integrates a fast converged iterative least-squares phase gradient correction algorithm with a deep learning algorithm, resulting in fast and high-precision InSAR phase unwrapping results in complex mountainous regions. The Dongchuan district of Kunming, Yunnan province, was chosen as the study area. The study area exhibits diverse land cover, including rocks, grasslands, and forests. The complex and mountainous terrain and the large gradient variation pose significant challenges to the InSAR phase unwrapping process. This problem is particularly evident in the studied regions, where the complex topography and diverse types of land cover make it challenging to resolve scattered objects, resulting in high noise levels in the InSAR phase. Large gradient variation also increases the likelihood of phase unwrapping, leading to incorrect results. Accurate phase unwrapping is thus particularly challenging in this regime, ultimately providing a demonstration application to regions of high noise and large gradient variation in complex mountainous areas.

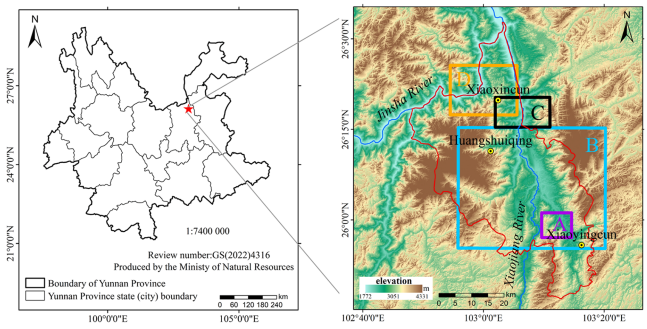

Fig. 1. Overview of the study area. We are featuring the location of the study area in Yunnan Province, China (marked with a red star) on the left side. The right panel displays the geographic location and topography of the study area, overlaid with the 30 m resolution DEM data. The red polygon outlines the study area, with zone A as a validation area for the SDPC unwrapping algorithm. Zones B, C, and D serve as training and validation sets for subsequent FPUNet networks.

II. Study Area and Datasets

A. Overview of Study Areas

Dongchuan is situated in the northernmost part of Kunming City in Yunnan Province, Southwest China. It is characterized by a longitude range of 102°47′-103°18′E and a latitude range of 25°46′-26°32′N. The region covers 1858.79 km^2, as Fig. 1 depicts. The average annual temperature is 14.9 °C, and the annual rainfall is around 1000 mm, primarily concentrated from May to October. Dongchuan stretches 84.6 km vertically from north to south and 51.2 km horizontally from east to west. The area is predominantly mountainous, constituting 97.3% of the total land, where the Jinsha and Xiaojiang rivers converge. The

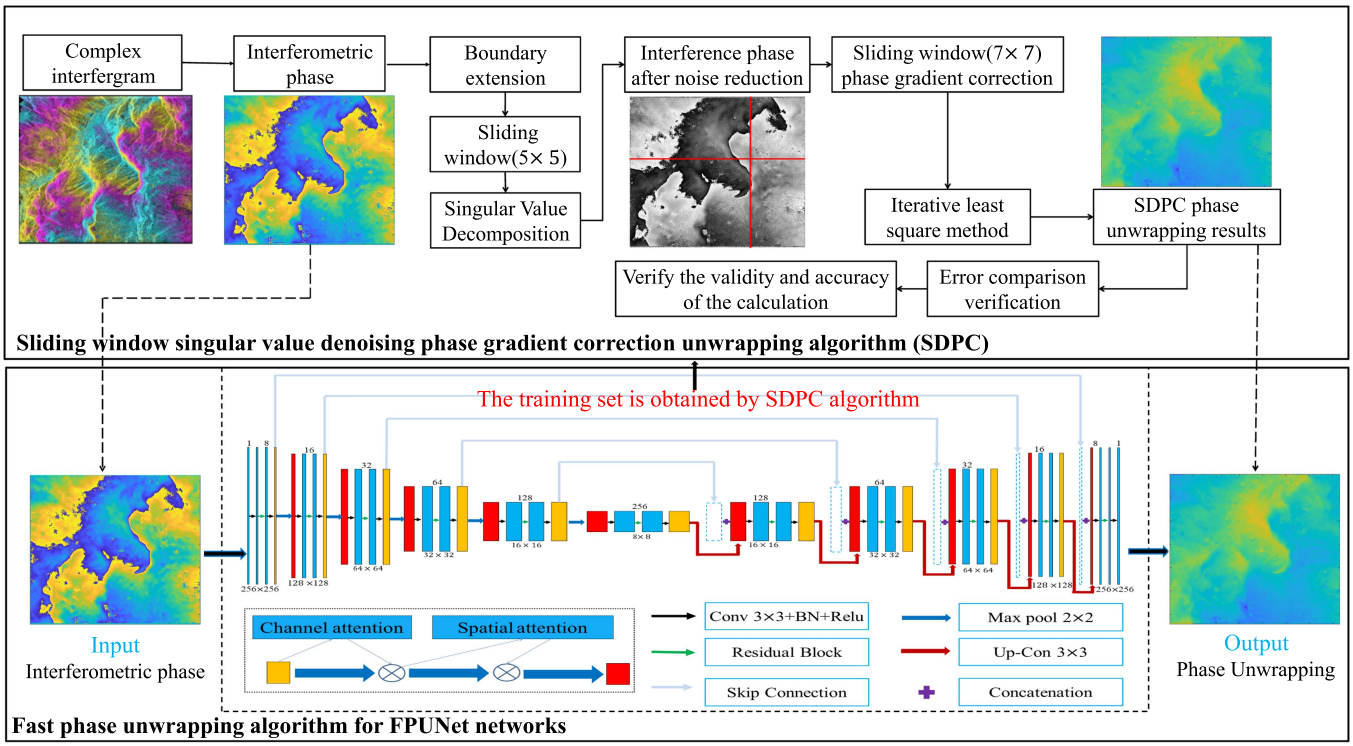

Fig. 2. Technical roadmap of the FPUNet phase unwrapping algorithm.

Xiaojiang River flows northwards, creating a "V" shape division. The highest peak reaches an elevation of 4344.1 m, and the terrain exhibits remarkable variations due to unique geological formations. Some regions encounter frequent heavy rainfall, leading to loose soil and significant erosion. Dongchuan is a globally important site for studying debris flows, often called the natural museum of debris flows.

B. Data

For this study, we acquired two sets of descending single look complex (SLC) images from the *C*-band Sentinel-1 Synthetic Aperture Radar (SAR) launched by the European Space Agency (ESA) in 2014. The first period spans from February 12 to February 24, 2023, while the second covers May 7 to May 19, 2023. The images were acquired in IW mode, *C*-band, and VV polarization, with a revisit period of 12 days. Preprocessing of the data included geocoding, registration, interferometry, and Goldstein filter using the GAMMA software, resulting in the corresponding interferometric phase data.

III. Method

This article introduces the FPUNet phase unwrapping algorithm, offering a solution for swift phase unwrapping in areas with elevated noise levels and significant gradient variations. Fig. 2 illustrates the technical roadmap of the FPUNet phase unwrapping algorithm. It consists mainly of two parts. The first step is a sliding window singular value denoising phase gradient correction unwrapping algorithm (SDPC). A sliding window (7 × 7) is applied for complex interferograms to obtain the singular value decomposition and the denoised complex interferogram. Then, a reference unwrapping point is selected, and a sliding window (15 × 15) is used to correct the phase gradient, avoiding the propagation of global errors. Finally, the number of iterations and the error are set, and the phase unwrapping is performed using ILS, followed by an accuracy evaluation comparing it with existing traditional phase unwrapping algorithms. Hence, the efficacy of the SDPC algorithm has been confirmed. The second step proposes a fast-phase unwrapping algorithm using the FPUNet network. The raw interferometric phase maps and the phase unwrapping results obtained using the SDPC algorithm are used to construct the dataset by computing the number of phases unwraps obtained as output data. Subsequently, the dataset is utilized to train the FPUNet network, leading to the acquisition of an FPUNet network model. Fast and efficient InSAR phase unwrapping can be achieved in large and complex mountainous regions with high noise and large gradient variations by inputting interferometric data and applying an FPUNet network model with specific postprocessing. The detailed steps of the algorithm are given below:

A. Sliding Window Singular Value Denoising Phase Gradient Correction Unwrapping Algorithm

The complex interference pattern can be represented as $s(r) = u(r)\exp(j\phi)$, with u representing s's amplitude and ϕ representing s's phase.

Suppose the size of the complex interference diagram is M × N, and the boundary is symmetrically extended by m pixels to avoid incomplete operation at the border. A local sliding window

with size $m \times m$ and the center ($m1$, $m1$) pixel is used to treat all the complex interference diagram pixels inside the window as a complex matrix $\mathbf{S}_{(m1,m1)}$

$$\mathbf{S}_{(m1,n1)} = \begin{bmatrix} \mathrm{S}_{i,k} & \mathrm{S}_{i,k+1} & \cdots & \mathrm{S}_{i,m} \\ \mathrm{S}_{i+1,k} & \mathrm{S}_{i+1,k+1} & \cdots & \mathrm{S}_{i+1,m} \\ \vdots & \vdots & \vdots & \vdots \\ \mathrm{S}_{m,k} & \mathrm{S}_{m,k+1} & \cdots & \mathrm{S}_{m,m} \end{bmatrix}. \quad (1)$$

The matrix singular value decomposition of $\mathbf{S}_{(m1,m1)}$ is denoted by

$$\mathbf{S}_{(m1,n1)} = \boldsymbol{U}_{\mathrm{S}} \boldsymbol{\Omega}_{\mathrm{S}} \boldsymbol{V}_{\mathrm{S}}^{T} \quad (2)$$

$$\boldsymbol{\Omega}_{\mathrm{S}} = \begin{bmatrix} \sigma_1 & 0 & \cdots & 0 \\ 0 & \sigma_2 & \cdots & 0 \\ \vdots & \vdots & \vdots & \vdots \\ 0 & 0 & \cdots & \sigma_m \end{bmatrix} \quad (3)$$

where the $\boldsymbol{\Omega}_{\mathrm{S}}$ in matrix $\sigma_{\mathrm{z}} = (z = 1, 2, \ldots, m)$ represents the computed singular values. $\boldsymbol{U}_{\mathrm{S}}$ and $\boldsymbol{V}_{\mathrm{S}}$ represent the left singular and proper singular matrix of $\mathbf{S}_{(m1,m1)}$.

After performing matrix singular value decomposition, the smaller distinct values are discarded to achieve the denoising effect, and the resulting denoised complex interference phase matrix $\mathbf{S}^{*}_{(m1,n1)}$is constructed as follows:

$$\left.\begin{aligned} \mathbf{S}^{*}_{(m1,n1)} &= \boldsymbol{U}_{S} \boldsymbol{\Omega}^{*}_{\mathrm{s}} \boldsymbol{V}_{S}^{T} \\ \boldsymbol{\Omega}^{*}_{\mathrm{s}} &= \begin{bmatrix} \sigma^{*} & 0 & \cdots & 0 \\ & & [\mathbf{0}]_{(m-5)\times(m-5)} & \end{bmatrix} \\ \sigma^{*} &= \sigma_1 - \tfrac{1}{m-5} \textstyle\sum_{z=m-3}^{m} \sigma_z \end{aligned}\right\} \quad (4)$$

where$[\mathbf{0}]_{(m-5)\times(m-5)}$ is the zero matrix, and σ^{*} is the principal component of the singular value.

According to the above method, the denoised complex interference diagram $\mathbf{S}^{*}_{(M,N)}$ is obtained using the sliding window to traverse the M $\times$ N complex interference diagram. $\phi = angle(\mathbf{S}^{*}_{(M,N)})$ can extract the interference phase from the complex interference pattern. A reference phase unwrapping point is chosen at the interference phase. The threshold for computing the wrapped phase gradient is calculated for each sliding window in $O \times P$ [23], [24]

$$\begin{cases} T_x = \sqrt{\mathrm{avg}\left[\left(\Delta^{x}_{hl}\right)^2\right] - \left(\mathrm{avg}\left[\Delta^{x}_{hl}\right]\right)^2} \\ T_y = \sqrt{\mathrm{avg}\left[\left(\Delta^{y}_{hl}\right)^2\right] - \left(\mathrm{avg}\left[\Delta^{y}_{hl}\right]\right)^2} \end{cases} \quad (5)$$

$$\begin{cases} G_x = \frac{1}{OP} \sum_{\mathrm{h}=0}^{h=O-1} \sum_{l=0}^{l=P-1} \Delta^{x}_{hl} \\ G_y = \frac{1}{OP} \sum_{\mathrm{h}=0}^{h=O-1} \sum_{l=0}^{l=P-1} \Delta^{y}_{hl} \end{cases} \quad (6)$$

where$\Delta^{x}_{hl}/\Delta^{y}_{hl}$ represents the estimated phase gradient in the horizontal/vertical direction within the local sliding window, avg represents the mean calculation, T_x/T_y is the standard deviation of the phase gradient $\Delta^{x}_{hl}/\Delta^{y}_{hl}$ in the horizontal/vertical direction within the local sliding window, G_x/G_y is the average value of the phase gradient $\Delta^{x}_{hl}/\Delta^{y}_{hl}$ in the horizontal/vertical direction within the local sliding window.

It replaces the phase gradient value larger than the standard deviation T_x/T_y within a local window with the mean value of the phase gradient G_x/G_y. Use a sliding window to traverse the entire M $\times$ N interferogram in pixel size according to the above method, completing the correction of the wrapped phase gradient.

The fundamental concept behind the ILS method involves utilizing phase quality information as a weight to minimize the discrepancy between the true and wrapped phase gradients. Considering a wrapped phase map of size M $\times$ N, where $\phi_{i,j}$ represents the wrapped phase, and $\varphi_{i,j}$ denotes the unwrapped phase obtained through phase unwrapping, the cost function C can be expressed as follows [18], [25]:

$$\begin{aligned} J = &\sum_{i=0}^{X-2} \sum_{j=0}^{Y-1} R_{i,j} \left|\varphi_{i+1,j} - \varphi_{i,j} - \Delta^{x}_{i,j}\right|^2 \\ &+ \sum_{i=0}^{X-1} \sum_{j=0}^{Y-2} C_{i,j} \left|\varphi_{i,j+1} - \varphi_{i,j} - \Delta^{y}_{i,j}\right|^2 \end{aligned} \quad (7)$$

$$\begin{cases} \Delta^{x}_{i,j} = w\left\{\phi_{i+1,j} - \phi_{i,j}\right\} \\ \Delta^{y}_{i,j} = w\left\{\phi_{i,j+1} - \phi_{i,j}\right\} \end{cases} \quad (8)$$

where$\Delta^{x}_{i,j}$ and $\Delta^{y}_{i,j}$ denote the interferometric phase differences in the horizontal and vertical directions x and y, respectively, where i ranges from 0 to *M-1*; j ranges from 0 to *N-1*;$w\{\cdot\}$ denotes the phase wrapping operator; $R_{i,j}$ and $C_{i,j}$ correspond to the weight parameters, which can be derived from the quality information of the interferogram $Z_{i,j}$

$$\begin{cases} R_{i,j} = \min\left[Z^2_{i+1,j}, Z^2_{i,j}\right] \\ C_{i,j} = \min\left[Z^2_{i,j+1}, Z^2_{i,j}\right] \end{cases} 0 \le Z^2_{i,j} < 1. \quad (9)$$

When the cost function J is minimized, the wrapped phase gradient is introduced, and then it satisfies the following:

$$\begin{aligned} \ell_{i,j} = &R_{i,j} \cdot \Delta^{x}_{i,j} - R_{i-1,j} \cdot \Delta^{x}_{i-1,j} \\ &+ C_{i,j} \cdot \Delta^{y}_{i,j} - C_{i,j-1} \cdot \Delta^{y}_{i,j-1} \end{aligned} \quad (10)$$

where $\ell_{i,j}$ is the Laplacian function used to represent the phase-weighted value.

The unwrapped phase $\varphi_{i,j}$ can been obtained through multiple iterations of the Gauss–Seidel relaxation method

$$\varphi_{i,j} = \frac{R_{i,j}\varphi_{i+1,j} + R_{i-1,j}\varphi_{i-1,j} + C_{i,j}\varphi_{i,j+1} + C_{i,j-1}\varphi_{i,j-1} - \ell_{i,j}}{R_{i,j} + R_{i-1,j} + C_{i,j} + C_{i-1,j}} \quad (11)$$

According to equation (11) iterates continuously to compute the discrepancy between the current and previous unwrapped phases. The phase unwrapping process concludes when the discrepancy falls below a specific threshold. By incorporating the corrected wrapped phase gradient into the ILS algorithm defined

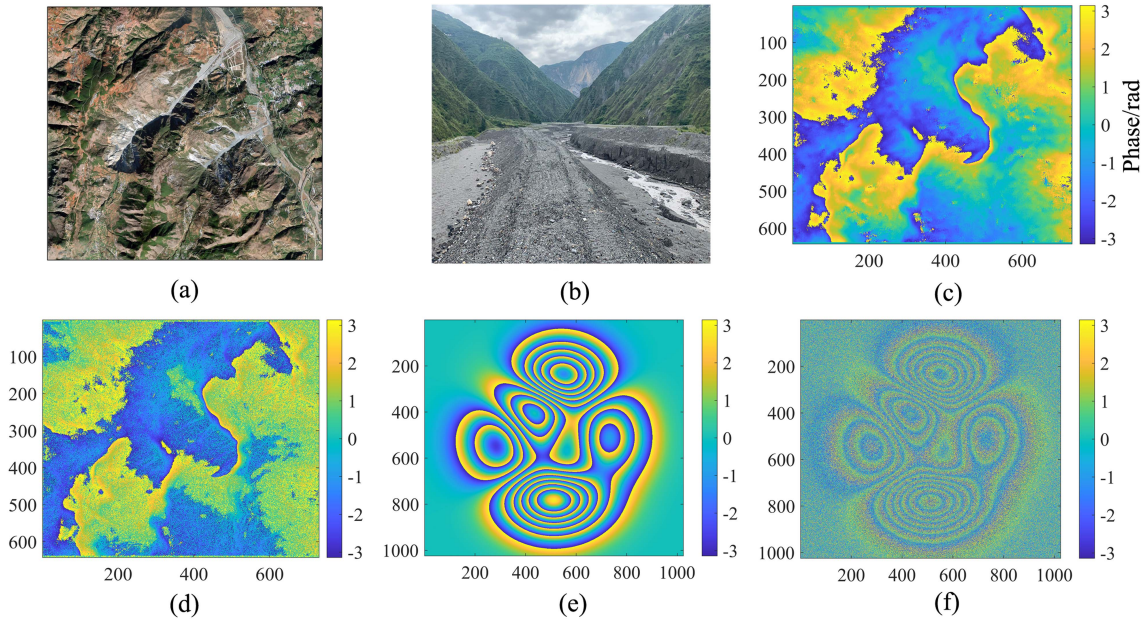

Fig. 3. Optical images and field survey photographs of region A, together with simulated interferometric data. (a) Google optical image of area A. (b) Field survey photo of area A. (c) Interferometric phase of area A. (d) High noise interferometric phase of area A. (e) Simulated interferometric phase without noise. (f) Simulated interferometric phase with high Gaussian noise. (a) Optical image. (b) Field survey photo. (c) Original noise phase. (d) High noise phase. (e) Phase without noise. (f) Phase with high Gaussian noise.

in (11), the SDPC algorithm accomplishes phase unwrapping and yields the final unwrapped phase outcome.

Area A, consisting of a pixel size of 642 × 730, was chosen to validate the proposed SDPC phase unwrapping algorithm. Fig. 3(a) and (b) display an optical image and a field photograph of area A, respectively, featuring two distinctive debris flow channels characterized by rugged terrain and significant undulations. During the phase unwrapping process, features such as large changes in the phase gradient exist. The SDPC phase unwrapping algorithm was applied to acquire the phase unwrapping outcomes for the region under consideration. Additionally, SDPC was employed to unwrap the interferometric phase prior to filtering, thereby evaluating the feasibility and effectiveness of utilizing Singular Value Decomposition for denoising within the SDPC phase unwrapping algorithm. Fig. 3(c) illustrates the interferometric phase of area A, while Fig. 3(d) displays the interferometric phase with added high Gaussian noise, having a standard deviation of 0.06, to the original interferometric phase for the same area. Considering that real measured data cannot obtain the true results of phase unwrapping, for this reason, through simulation and simulated data, the mean absolute error was used to verify the phase unwrapping accuracy of different unwrapping algorithms (BC; ILS MCF; the proposed SDPC method). The noise was added to ensure fairness and was Gaussian with a standard deviation 0.8. In order to validate the effectiveness of various phase unwrapping algorithms in high-noise areas, simulation data was generated using the Peaks function. Fig. 3(e) and (f) depicts the simulated interferometric phase without noise and the simulated interferometric phase with added Gaussian noise, having a standard deviation of 0.8, respectively.

B. FPUNet: Fast Phase Unwrapping Method Based on SDPC

The fast-phase unwrapping method, which relies on SDPC, is derived from the phase unwrapping outcomes obtained by employing the sliding window singular value corrected model for phase gradient correction and unwrapping, known as SDPC. Equation (12) demonstrates the connection between the unwrapped and wrapped phases. Utilizing the measured interferometric phase and the number of phase wraps, we propose a rapid InSAR phase unwrapping approach based on the FPUNet network model

$$\varphi = \phi + 2\pi k\,(x) \tag{12}$$

where φ represents the unwrapped phase, ϕ signifies the wrapped phase, and $k(x)$ is an integer that denotes the number of wrapped phases.

C. Network Structure

U-Net is a widely utilized deep learning network architecture in image semantic segmentation tasks [26], [27] and is considered a mainstream technology for image semantic segmentation [28], [29]. The proposed FPUNet network in this article incorporates a residual network [30] and a convolution block attention module (CBAM) [31] into the U-Net [32]. Fig. 4 illustrates its network structure, including encoding, decoding, and bridging paths. The encoding path consists of five modules that progressively extract semantic features from the interferogram. Each submodule includes 3 × 3 convolution operations (followed by BN [33] and ReLU [34], as well as a 2 × 2 max pooling operation. The initial convolution operation enhances the number

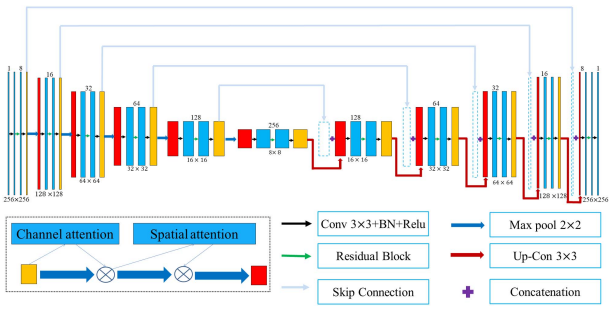

Fig. 4. Network model structure of FPUNet, where the arrows and symbols indicate different operations.

of feature channels in each submodule, using eight convolution kernels to increase the channels from one to eight. Subsequently, the number of channels in each submodule is doubled.

The bridging path excludes the max pooling operation from the encoded path. Each step of the decoding path includes a deconvolution, a skip connection, 3×3 convolution operations (followed by BN and ReLU), and a residual block positioned between these convolutions. During each iteration of the decoding path, the two convolution operations decrease the number of feature channels (except for the last iteration, which reduces the channels from 8 to 1). The residual block and skip connection can accelerate the convergence of the network, extract richer interferometric phase features, and prevent gradient diffusion and gradient explosion. Convolutional block attention modules, consisting of channel and spatial attention modules, are incorporated during the upsampling process in the encoding path and the downsampling process in the decoding path. The channel attention module enables selective enhancement or suppression of individual channels by learning channel-specific weights. During downsampling, the channel attention module helps the CNN model choose the most relevant channels to reduce redundant information and computational complexity. During upsampling, it can help the model capture more details and textures. The spatial attention module selectively emphasizes or suppresses different locations by learning the weights of each pixel. During downsampling, the spatial attention module can help the model capture a wider range of contextual information to improve its perception and understanding capabilities. During upsampling, it can help the model reconstruct details and textures more effectively. The FPUNet network consists of 49 convolutional and deconvolutional layers. The encoding path converts input information into a higher level and more abstract feature space.

In contrast, the decoding path converts the abstract and high-level information into a representation in the output space, establishing a mapping between the interferometric phase (wrapped phase) and the phase-wrapped number format. During network training, the average cross-entropy loss function is employed as the loss function, and the Adam optimizer is utilized to optimize the network parameters [35]. The FPUNet network takes raw complex interferograms with varying noise levels as inputs and generates phase-wrapped number results corresponding to the complex interferograms. The training parameters of the FPUNet network are updated by minimizing the loss function.

D. Data Generation

For the training set (Region B) and validation sets (Regions C and D) in the network model of FPUNet, the interferometric phase is extracted from the obtained actual complex interferograms, Gaussian noise with different standard deviations is added, and the corresponding phase unwrapping results are obtained using the SDPC algorithm. According to (12), the corresponding phase-wrapped number is obtained. The interferometric phase and the corresponding phase-wrapped number are segmented into 256×256 pixel sizes, with the size of each pixel in the training set (Region B) being 3119×3959. They are divided into 3,808 groups with a 50% overlap. The pixel size of the validation set (Region C) is 840×1454, divided into 24 groups in order. The pixel size of the validation set (Region D) is 1304×1273, divided into 30 groups in order. Fig. 5(a) and (c) display the interferometric phase of the measured data in Region C. In contrast, Fig. 5(b) and (d) exhibits the corresponding unwrapped phase achieved through the SDPC unwrapping algorithm. Additionally, Fig. 5(e) and (f) presents the segmented interferometric and unwrapped phases with pixel sizes of 256×256.

In practical applications, obtaining the ideal unwrapped phase corresponding to the measured noisy interferometric phase is difficult. Therefore, it is necessary to introduce simulated data to generate many noisy interferometric phases and related unwrapped phases to meet the sample requirements for network training. The steps for generating simulated data are: first, random matrices of different sizes, such as 2×2 and 8×8, are recommended for resolution. Next, the bilinear interpolation method is used to expand the above random matrices to a 256×256 pixel matrix, and their values are amplified to obtain a real phase without wrapping. Finally, noisy interferometric phase maps with different S/N ratios are obtained by adding other noises, and their corresponding phase-wrapped numbers are obtained through (12). Three thousand datasets are generated as the training set [34], [36]. Fig. 5(g) and (h) shows the simulated 256×256 pixel interferometric phase and phase-wrapped number.

Using the constructed FPUNet network, the above 6808 training datasets are learned and trained. The learning process consists of 250 epochs with a batch size of 32 and a learning rate of 0.01. The weight values are obtained by learning and training and saved. The trained FPUNet network obtains the phase-wrapped number of the measured Regions C and D with a pixel size of 256×256 under different noises. The unwrapped phase is calculated based on (12), and by merging the segmented 256×256 unwrapped phases, the final complete unwrapped phase is obtained after combining Regions C and D.

E. Postprocessing, Accuracy, and Efficiency Evaluation of the Unwrapping Results

Promising preliminary results can be obtained using deep learning for phase estimation in phase unwrapping. However, postprocessing techniques are often necessary to enhance the quality of the results, addressing challenges such as noise, artifacts, discontinuities, incompleteness, global consistency,

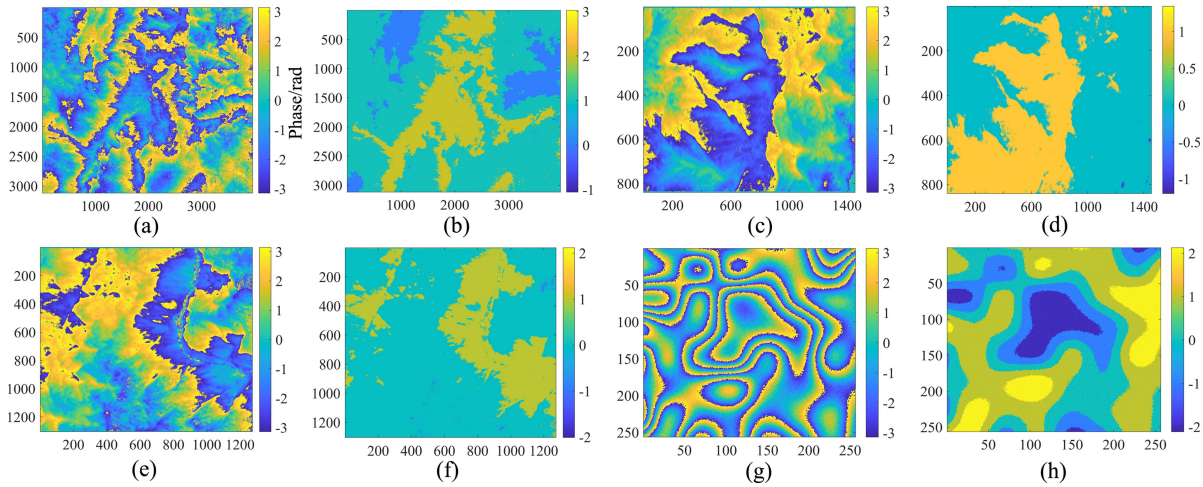

Fig. 5. Interferometric phase and the number of phase envelopes. (a), (c), and (e) Measured interferometric phases in Regions B, C, and D, respectively. (b), (d), and (f) Corresponding phase-wrapped numbers. (g) and (h) Simulated 256 × 256 pixel interferometric phases and phase-wrapped numbers. (a) B interferometric. (b) B phase-wrapped numbers. (c) C interferometric phase. (d) C phase-wrapped numbers. (e) D interferometric phase. (f) D phase-wrapped numbers. (g) Interferometric phase. (h) Phase-wrapped numbers.

and edge and detail preservation. Postprocessing methods can repair and improve the phase image, making it more consistent with the true phase and improving the accuracy and stability of unwrapping. This article's phase value error obtained by deep learning based on the original 256 × 256 pixel interferometric phase is correct using the phase unwrapping result obtained from the SDPC unwrapping algorithm. Iterative least-squares correction is used to gradually reduce the part of the phase that cannot be accurately predicted by the deep learning model, thus enhancing the quality of the phase unwrapping outcomes.

As the true phase information of the actual measured data is unavailable, we utilize the simulated data, which contains both the interferometric phase and the true unwrapped phase, to assess the accuracy of the FPUNet unwrapping outcomes. The evaluation compares the mean absolute and root-mean-square errors with the SDPC unwrapping results using the noisy simulated data.

To evaluate the efficiency of FPUNet in phase unwrapping, we chose Region D of the validation set as the experimental object. The efficiency of different unwrapping algorithms, such as BC, ILS, MCF, SDPC, and FPUNet, was assessed by analyzing the execution time on a computer device equipped with an Intel(R) Xeon(R) Silver 4210R CPU @2.40 GHZ, 128 GB of memory, and an NVIDIA GeForce RTX 3090 graphics card.

IV. Results and Analysis

A. SDPC Phase Unwrapping Results and Verification Results of Different Unwrapping Algorithms

Fig. 6 shows the validation results of different phase unwrapping algorithms under simulated data. Fig. 6(d) reflects some extent, the character of large gradient change in analog simulation data, with the highest phase value of 40 rad. Fig. 6(e) shows that different phase unwrapping algorithms can successfully

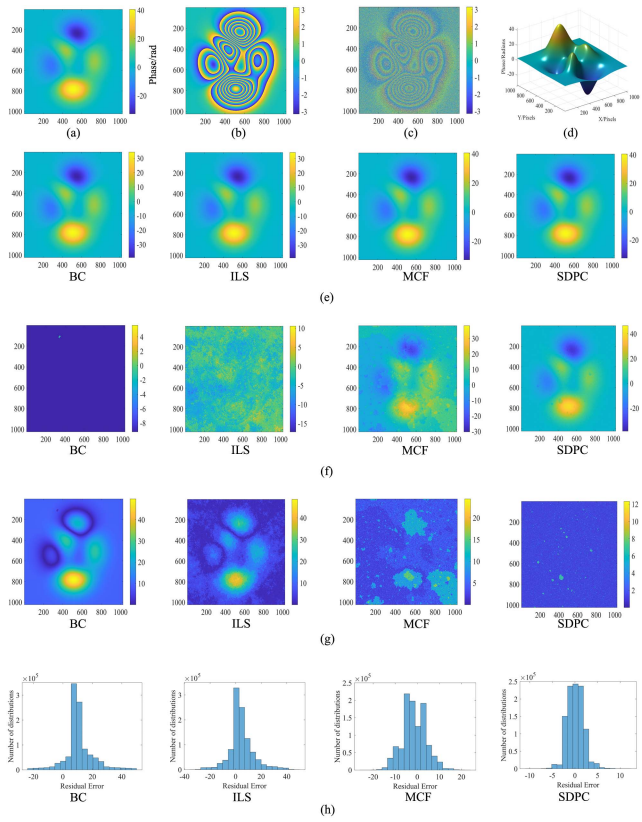

Fig. 6. Verification results of different phase unwrapping algorithms under simulated data. (a) and (b) True and interferometric phases under noiseless conditions. (c) High noise interferometric phase generated using the Peaks function. (d) Three-dimensional phase unwrapping result. (a) True phase. (b) Noiseless interference phase. (c) High noise interference phase. (d) 3D phase. (e) Results of different unwrapping algorithms without noise conditions. (f) Results of different unwrapping algorithms for high noise conditions. (g) Absolute error of different unwrapping algorithms under high noise conditions. (h) Residuals of different unwrapping algorithms under high noise conditions.

TABLE I
MEAN ABSOLUTE ERROR AND ROOT-MEAN-SQUARE ERROR OF DIFFERENT PHASE-UNROLLING ALGORITHMS UNDER SIMULATED DATA

Noise condition	Evaluation index	Phase unwrapping algorithm			
		BC	ILS	MCF	SDPC
Noiseless	MAE	6.411	6.283	0.001	0.002
	RMSE	6.729	6.283	0.020	0.043
High noise	MAE	12.259	7.230	4.543	1.417
	RMSE	14.572	10.412	5.576	1.782

unwrap the interference phase under the noise-free condition. The corresponding evaluation indicators for phase unwrapping errors are presented in Table I. The BC method exhibits the largest average absolute and mean square errors measuring 6.411 and 6.729 rad, respectively. The MCF method demonstrates relatively lower average absolute error and mean square error, with values of 0.001 and 0.020 rad, respectively. The proposed SDPC phase unwrapping algorithm in this study achieves significantly higher precision in terms of average absolute error and mean square error compared to the BC method and the ILS method but slightly lower precision than the MCF method. It is due to the introduction of the singular value decomposition for noise reduction in the SDPC phase unwrapping algorithm, which to some extent, removes the low interference phase feature for the noiseless interference phase, resulting in this situation. However, in practical applications, the interferometric phase obtained by InSAR processing cannot be noise-free. Hence, analyzing and discussing the accuracy of phase unwrapping in scenarios with high noise and large gradients is more realistic and meaningful. From Fig. 6(f), it can be seen that under high noise conditions, for regions with large gradient changes, the phase unwrapping result obtained by the SDPC method is closer to the true phase. The MCF method performs well in flat areas but is less effective in high-relief or low-lying areas. Although the ILS method can perform phase unwrapping, its result cannot reflect the true phase. The BC method is powerless in high-noise and large-gradient regions and cannot obtain the final phase unwrapping result. The reason is that in the high noise region, the branch-and-cut method is prone to spurious gradients, that is, incorrect gradient directions. At the same time, when the phase changes dramatically, there can be discontinuities in the gradient direction, leading to inaccurate phase unwrapping at the gradient change. Fig. 6(g) shows different phase algorithms' corresponding absolute error distribution maps.

The SDPC method outperforms the other three-phase unwrapping methods (BC, ILS, and MCF) with a significantly lower average absolute error of 1.417 rad and root-mean-square error of 1.782 rad. Fig. 6(h) shows the residual distribution statistics of different phase unwrapping algorithms under high-noise conditions. The residual of the BC method mainly ranges from 5 to 13 rad, the residual of the ILS method mainly ranges from -1 to 7 rad, the residual of the MCF method mainly ranges from -6 to 4 rad, and the residual of the SDPC method mainly ranges from -2.81 to 3.04 rad. The SDPC method has a smaller main residual range and higher precision. In summary, the simulation data confirms that the SDPC method surpasses other phase unwrapping methods in terms of efficiency and accuracy when dealing with regions characterized by high noise and large gradient variations.

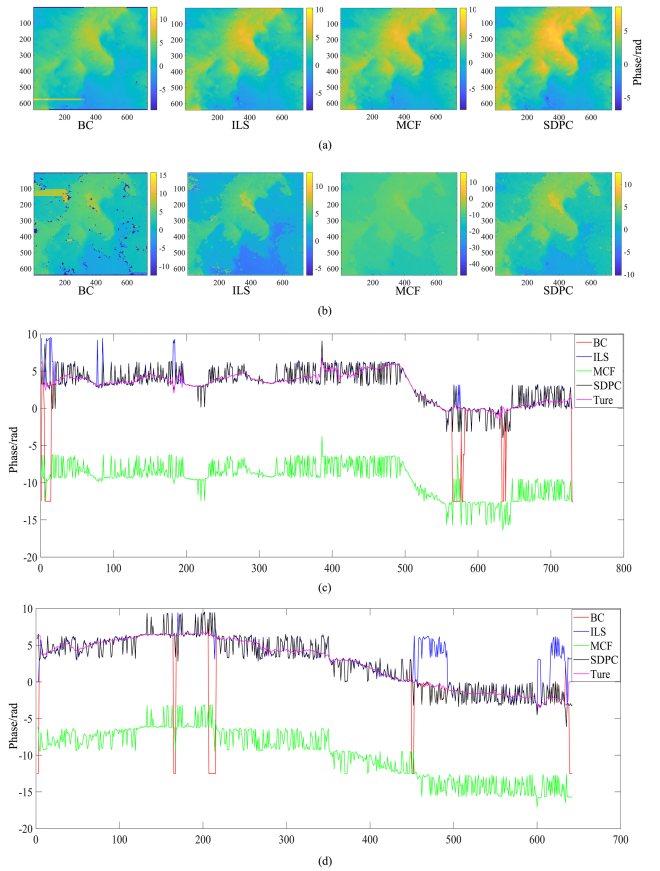

Fig. 7. Results and similarity curves for different phase unwrapping algorithms in region A. (a) Results of different unwrapping algorithms original noise conditions. (b) Results of different unwrapping algorithms for high noise conditions. (c) Similarity curves of different unwinding algorithms and truth values in column directions. (d) Similarity curves of different unwinding algorithms and truth values in row directions.

The simulated data above confirms the superior efficiency and accuracy of the SDPC method compared to other methods in regions with high noise and large gradient variations. Using the SDPC algorithm, the phase unwrapping result of the original interferometric phase in area A with noise is considered the ground truth for evaluating the performance in high-noise and large-gradient regions of area A. Fig. 7 shows the results and similarity curves of different phase unwrapping algorithms in study area A. Fig. 3(c) displays the interferometric phase in area A, while Fig. 3(d) shows the high-noise interferometric phase resulting from adding noise to the original interferogram. In Fig. 7(a), the phase unwrapping results of the BC method under the original noise condition appear unsatisfactory, while the other phase unwrapping results exhibit relatively consistent performance. Table II presents the mean absolute and root-mean-square errors of the three phase unwrapping algorithms compared to the SDPC algorithm. Among them, the MCF algorithm outperforms the ILS and BC algorithms in the presence of raw noise. Fig. 8(b) showcases the results of different phase unwrapping algorithms in area A under high noise conditions.

TABLE II
MEAN ABSOLUTE ERROR AND ROOT-MEAN-SQUARE ERROR FOR DIFFERENT PHASE-FREE ROLLING ALGORITHMS IN REGION A

Noise condition	Evaluation index	Phase unwrapping algorithm			
		BC	ILS	MCF	SDPC
Original noise	MAE	0.224	0.014	0.013	0.000
	RMSE	1.425	0.158	0.152	0.000
High noise	MAE	1.491	1.153	12.581	1.417
	RMSE	3.221	1.921	12.663	1.782

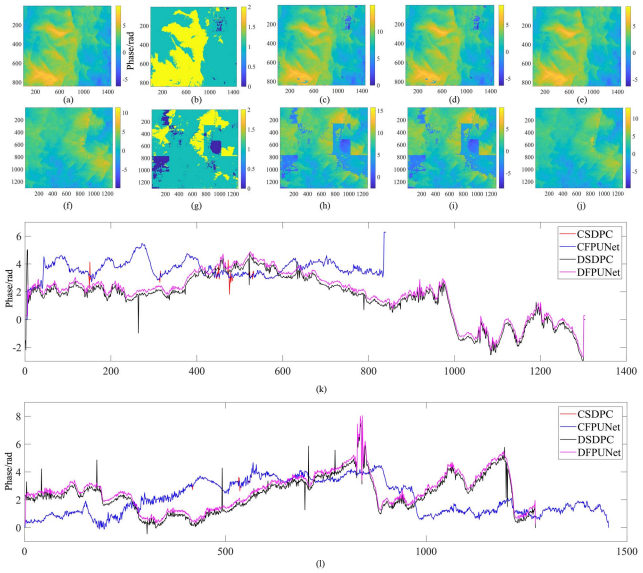

Fig. 8. FPUNet phase unwrapped results and similarity curve chart for regions C and D. (In the legend, "CSDPC " represents the curve obtained by the SDPC unwrapping algorithm in region C, "CFPUNet" represents the curve obtained by FPUNet unwrapping algorithm in region C, "DSDPC " and "DFPUNet" represent the curves obtained by SDPC and FPUNet unwrapping algorithms in region D, respectively). (a) C interference phase. (b) C phase-wrapped numbers. (c) C wrapped phase. (d) C phase corrections. (e) C unwrapping correction. (f) D interference phase. (g) D phase-wrapped numbers. (h) D wrapped phase. (i) D phase corrections. (j) D unwrapping correction. (k) SWES and FPUNet unwrapping algorithms for regions C and D show the similarity curves in column direction. (I) SWES and FPUNet unwrapping algorithms for regions C and D show the similarity curves in row direction.

Notably, the SDPC method demonstrates low mean absolute and root-mean-square errors compared to the other three phase unwrapping algorithms. Fig. 7(c) and (d) depicts the similarity curves of different phase unwrapping algorithms in the row and column directions. It is apparent that, under high noise conditions, the BC and ILS methods exhibit some rough consistency with the true curve but with numerous significant deviations. The similarity curve of the SDPC method is the closest to the true curve without large jump bias, while the similarity curve of the MCF method is far from the true curve. It is because all weights are set to the default value of 0.5, which partly reflects the fact that the accuracy of the MCF method is hardly guaranteed in regions of high noise and large gradient variations due to the difficulty in determining unbiased coherence and other weight factors. In summary, this study has confirmed that the SDPC phase unwrapping algorithm is effective in regions of high noise and large gradient variations in region A, providing a dataset

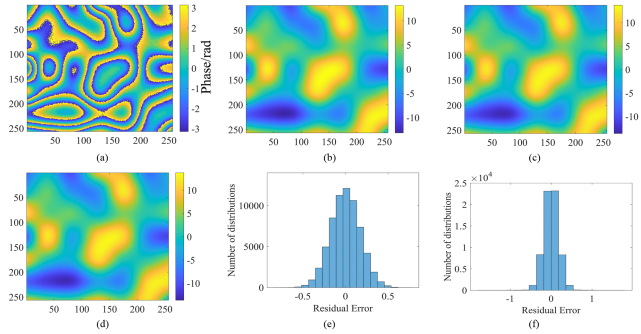

Fig. 9. FPUNet phase unwrapping results and residual maps for simulated data with noise. (a) Phase with noise. (b) True phase. (c) FPUNet unwrapping phase. (d) SDPC unwrapping phase. (e) FPUnet residual error. (f) SDPC residual error.

to support the subsequent implementation of fast and accurate InSAR phase unwrapping using the FPUNet network.

B. FPUNet Phase Unwrapping Results and Accuracy Evaluation

Fig. 8 shows the results of FPUNet phase unwrapping on validation sets C and D. Fig. 8(b) and (g) shows the wrapped phase obtained by FPUNet in C and D regions. Fig. 8(e) and (h) displays the phase unwrapping results obtained by FPUNet using (12). The unwrapped outcomes generated by FPUNet exhibit several discontinuous areas that necessitate postprocessing. Fig. 8(d) and (i) shows the corrected phase values obtained using SDPC unwrapping algorithm based on the original 256 × 256 pixel interferometric phase in C and D regions to correct the phase errors obtained by FPUNet. Fig. 8(e) and (j) depicts the postprocessed results achieved by applying the ILS method to the unwrapped phase obtained from FPUNet in regions C and D. From a visual perspective, the results of Fig. 8(e) and (j) are consistent with those obtained by SDPC. Combining the similarity curve charts of SDPC and FPUNet in column and row directions of Fig. 8(k) and (l), it can be seen that for region C, the similarity curves obtained by SDPC and FPUNet are consistent, and the similarity curve generated by FPUNet has no major mutations. For region D, the sequences of similarity curves obtained by SDPC and FPUNet are roughly consistent but not identical. The similarity curve obtained by SDPC has substantial variations, while the similarity curve obtained by FPUNet is smoother. Incorporating a substantial volume of simulated data into the training sample set makes the outcome more inclined toward the true unwrapped phase result.

The above section discussed that SDPC has the best unwrapping results for noisy simulated data. Therefore, this section compares the phase unwrapping results and residual maps obtained by FPUNet and SDPC for noisy simulated data with noise. Fig. 9(a) displays the interferometric phase with noise, while Fig. 9(b) presents the true unwrapped phase. Fig. 9(c) and (d) shows the unwrapped phase results of FPUNet and SDPC, respectively. Visually, the results obtained by the two unwrapping algorithms are consistent with the true unwrapped phase. By comparing the residual maps in Fig. 9(e) and (f), it can

TABLE III
MEAN ABSOLUTE ERROR AND ROOT-MEAN-SQUARE ERROR FOR DIFFERENT UNWRAPPING ALGORITHMS FOR SIMULATED DATA WITH NOISE

Evaluation index	Phase unwrapping algorithm	
	FPUNet	SDPC
MAE	0.137	0.139
RMSE	0.172	0.178

TABLE IV
TIME REQUIRED BY DIFFERENT UNWRAPPING ALGORITHMS

Evaluation index	Phase unwrapping algorithm				
	BC	ILS	MCF	SDPC	FPUNet
Time/s	42.670	2.5	26.200	60.000	8.975

be seen that the residual map generated by FPUNet is distributed roughly between -0.5 and 0.5.

In contrast, the residual map generated by SDPC is distributed between -1 and 1. To quantitatively describe the mean absolute error and the root-mean-square error of the two unwrapping algorithms, the results are shown in Table III. It can be seen that the results obtained by the FPUNet unwrapping algorithm are slightly better than those obtained by the SDPC unwrapping algorithm. It also demonstrates that using the FPUNet network to unwrap real measured data can generate smoother similarity curves without significant mutation.

Table IV shows the unwrapping time required by the different unwrapping algorithms for region D. Among them, the ILS algorithm takes the least time, which is 2.5 s, but it does not effectively guarantee the unwrapping accuracy. In contrast, the SDPC algorithm takes the longest time, up to 60 s. The BC algorithm requires 42.670 s unwrapping time, the MCF algorithm needs 26.200 s, and the FPUNet unwrapping algorithm requires only 8.975 s. Although it is not the fastest compared to ILS, its robust performance in high noise and large gradient regions demonstrates its ability to ensure both unwrapping accuracy and processing efficiency.

V. DISCUSSION

A. Advantages of Our Proposed Method Over Existing Methods in This Article

This article proposes the SDPC algorithm, a sliding window singular value correction model phase gradient correction unwrapping algorithm. It addresses the issue of inaccurate phase unwrapping in complex mountainous areas with high noise and large gradient changes. By utilizing a sliding window singular value decomposition, this algorithm effectively mitigates the impact of noise on the unwrapping results. In addition, it corrects the phase gradients in large gradient regions with a sliding window and finally obtains the phase unwrapping results using an ILS method. Building upon the SDPC unwrapping algorithm, we incorporate deep learning techniques and present the FPUNet network, a rapid InSAR phase unwrapping algorithm. This

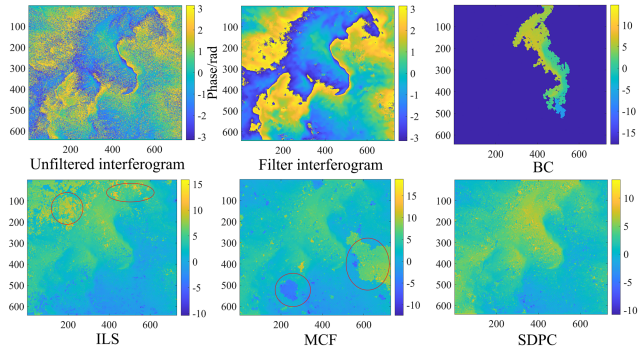

Fig. 10. Unwrapped results of unfiltered interferometric phase under different phase unwrapping algorithms.

network falls into the category of two-step unwrapping, which has higher unwrapping accuracy and better processing capability for complex scenes and large gradient regions than one-step unwrapping. The unwrapping speed can be further accelerated by harnessing the advantages of deep learning while maintaining unwrapping accuracy. According to the experimental results presented in this article, our proposed unwrapping algorithm can perform phase unwrapping accurately and efficiently in regions of high noise and large gradient variations compared to existing unwrapping methods for phase.

Moreover, based on deep learning, it can quickly and efficiently unwrap the interferometric phase over a large area. Unlike previous phase unwrapping algorithms based on deep learning frameworks, which only demonstrate their effectiveness on simulated data and small regions of size 256×256 pixels, our proposed method can handle real measured data over a large area. In addition, we summarize a set of postprocessing methods for deep learning-based phase unwrapping suitable for high noise and large gradient changing regions, including phase value correction and discontinuous phase correction using ILS methods. In summary, the proposed method effectively solves the problem of fast InSAR phase unwrapping for complex mountainous regions with high noise and large gradient variations. These advantages enable our proposed method to achieve higher unwrapping accuracy and faster processing in complex mountainous areas, providing significant value and potential for practical applications.

B. Evaluation of the Unwrapping Performance of the SDPC Algorithm Compared to Unwrapping of Unfiltered Interferometric Phase

The SDPC unwrapping algorithm applies to phase unwrapping in regions with high noise and significant gradient variations. However, all interferometric phase data used in this study were denoised using the Goldstein filter. It is still being determined whether our SDPC unwrapping algorithm performs better for unwrapped unfiltered interferometric phase data. To this end, the unfiltered interferometric phase of Zone A is obtained and unwrapped using different phase unwrapping algorithms. The results are shown in Fig. 10. The unfiltered phase is more noisy compared to the filtered interferometric phase. From the

TABLE V
MEAN ABSOLUTE ERROR AND ROOT-MEAN-SQUARE ERROR OF UNFILTERED INTERFEROMETRIC PHASE UNDER DIFFERENT PHASE UNWRAPPING ALGORITHMS

Evaluation index	Phase unwrapping algorithm			
	BC	ILS	MCF	SDPC
MAE	17.989	1.423	1.438	0.873
RMSE	18.907	2.356	2.439	1.327

perspective of the unwrapped images obtained, the BC algorithm cannot perform phase unwrapping efficiently. Although the ILS algorithm can achieve phase unwrapping overall, numerous inaccuracies and conflicted regions exist, as shown by the highlighted sections in red circles in Fig. 10.

Similarly, the MCF algorithm has inaccurate regions. The SDPC algorithm demonstrates superior efficiency in unwrapping the unfiltered interferometric phase, yielding results that closely resemble the SDPC unwrapped phase results shown in Fig. 7. The quantitative evaluation of the different phase unwrapping algorithms uses the mean absolute and root-mean-square errors, as shown in Table V. SDPC achieves the lowest mean absolute error of 0.873 rad and root-mean-square error of 1.327 rad. The mean absolute and root-mean-square errors obtained by ILS and MCF are comparable, while the BC algorithm exhibits the poorest performance. The quantitatively evaluated results are consistent with the qualitative analysis in Fig. 10, which further proves that the proposed SDPC algorithm can effectively unwrap unfiltered interferometric phase in areas with high levels of noise and large gradient changes and also demonstrates that the sliding window singular value decomposition proposed in the SDPC algorithm can effectively filter out the noise in interferometric phase.

C. Evaluation of the Phase Unwrapping Performance of FPUNet Compared to the Traditional ResUNet

Compared to the widely used ResUNet network model for phase unwrapping [37], this article's proposed FPUNet network model adds a convolutional block attention module to the ResUNet model. To explore whether FPUNet with the added convolutional attention module has certain advantages over ResUNet in the field of phase unwrapping, with the training set, learning parameters epochs, batch size, learning rate, and other parameters being consistent, phase wrapping numbers were obtained for validation set Zone D, and postprocessing was performed to evaluate the phase unwrapping accuracy of the two networks. The results show that the FPUNet phase unwrapping has a mean absolute error of 0.329 rad, which is 0.005 rad better than the ResUNet results, as shown in Table VI. The FPUNet phase unwrapping has a root-mean-square error of 0.558 rad, which is 0.028 rad better than the ResUNet phase unwrapping result. The above quantitative statistics show that the proposed FPUNet network with added convolutional block attention module achieves better phase unwrapping results than the existing conventional ResUNet network. The above ResUNet networks all utilize the

TABLE VI
COMPARISON OF MEAN ABSOLUTE ERROR AND ROOT-MEAN-SQUARE ERROR OF PHASE UNWRAPPING BETWEEN FPUNET AND TRADITIONAL RESUNET

Evaluation index	Phase unwrapping algorithm		
	FPUNet	ResUNet	ResUNet (No postprocessing)
MAE	0.329	0.334	2.309
RMSE	0.558	0.586	3.381

TABLE VII
COMPARISON OF MEAN ABSOLUTE ERROR AND ROOT-MEAN-SQUARE ERROR OF PHASE UNWRAPPING BETWEEN FPUNET AND TRADITIONAL SIMULATION DATA RESUNET

Evaluation index	Phase unwrapping algorithm	
	FPUNet	ResUNet
MAE	0.329	10.279
RMSE	0.558	10.806

postprocessing method in this article. We calculate the average absolute and root-mean-square errors of the phase unwrapping obtained by the ResUNet network without postprocessing. We can see from Table VI that the average absolute error and the root-mean-square error of the postprocessed ResUNet network have been reduced by 1.975 and 2.795 rad, which, to some extent, proves the effectiveness and advantage of the postprocessing method proposed in this article.

Since the training set used in the above ResUNet network is obtained from the SDPG algorithm in FPUNet network and also utilises the postprocessing method proposed by the FPUNet network, the average absolute error and root-mean-square error of phase unwrapping obtained using the ResUNet network are not much different from FPUNet network, however, for ResUNet network, many current deep learning phase unwrapping networks are using simulation data as a training set, for this reason, we use the simulation data will have been trained ResUNet network model, to phase unwrapping of the validation set D area, assessment to ensure that the phase unwrapping accuracy obtained by the two types of networks, and the results are shown in Table VII, the FPUNet phase unwrapping average absolute error is 0.329 rad, which is better than the ResUNet unwrapping result of 9.95 rad. The FPUNet phase unwrapping root-mean-square error is 0.558 rad, better than the ResUNet unwrapping result of 10.248 rad. It can be seen from the above quantitative statistics that our proposed FPUNet network is far better than the ResUNe network using simulation data.

D. Evaluation of Transferability and Generalizability of FPUNet Phase Unwrapping Algorithm

The mentioned studies utilized measured interferometric data acquired from processed *C*-band Sentinel-1 SAR radar SLC images, which the ESA captured between February 12 and February 24, 2023. However, in the realm of InSAR deformation monitoring, there is often a need to obtain long-term InSAR deformation results, as exemplified by existing techniques like

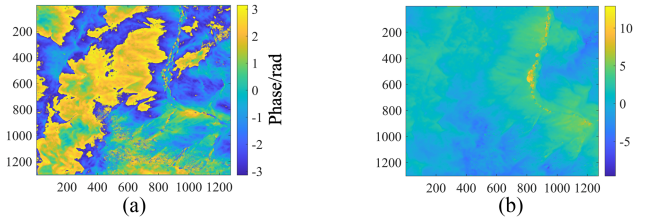

Fig. 11. Other time intervals of interferometric phase and FPUNet phase unwrapping results. (a) Interferometric phase. (b) Phase unwrapping results.

persistent scatterer-interferometric synthetic aperture radar (PS-InSAR) and small baselines subset-interferometric synthetic aperture radar (SBAS-InSAR). It means that the unwrapped phase information corresponding to different periods of the interferometric phase needs to be obtained. However, the training sample set of the FPUNet network needs to be constructed for each period of the interferometric phase. In that case, the efficiency of this approach in practical applications will be significantly reduced. Therefore, exploring the transferability and generalizability of the proposed FPUNet phase unwrapping algorithm is particularly important. To effectively evaluate the transferability and generalizability of the FPUNet phase unwrapping algorithm, we obtained individual complex images from May 7 to May 19, 2023. We used the GAMMA software to perform geocoding, registration, and interferometric preprocessing to obtain the corresponding interferometric phase data. Based on the FPUNet network model constructed in this article, we have received the corresponding unwrapped interferometric phase diagram for Zone A from May 7 to May 19, 2023, as shown in Fig. 11. Fig. 11(a) shows the measured interferometric phase obtained from May 7 to May 19, 2023, which differs from the estimated interferometric phase obtained from February 12 to February 24, 2023, shown in Fig. 5(e). The FPUNet phase unwrapping method also demonstrates rapid acquisition of the corresponding phase unwrapping result, as Fig. 11(b) depicts. This experiment indicates that the proposed method in this article eliminates the need for constructing a separate sample set specifically for time-series interferometric data, facilitating time-series interferometric phase unwrapping, effectively demonstrating that the FPUNet phase unwrapping algorithm has strong transferability and generalizability, which provides theoretical and technical support for the practical application of the proposed method.

E. Evaluation of One-Step Unwrapping Algorithm Effect of FPUNet Network

The one-step unwrapping approach has a significant advantage over the end-to-end approach, i.e., it learns all the steps between the input wrapping phase and the output unwrapping phase without any postprocessing procedure. In order to explore how effective the FPUNet network is using one-step unwrapping, keeping the training set, learning parameters epochs, batch size, learning rate and other parameters consistent with the method of this article, the number of phase wrapping is obtained for the validation set D area to evaluate the accuracy

TABLE VIII
COMPARISON OF MEAN ABSOLUTE ERROR AND ROOT-MEAN-SQUARE ERROR OF ONE-STEP AND TWO-STEP PHASE UNWRAPPING

Evaluation index	Phase unwrapping algorithm	
	FPUNet (two-step)	FPUNet (one-step)
MAE	0.329	10.279
RMSE	0.558	10.806

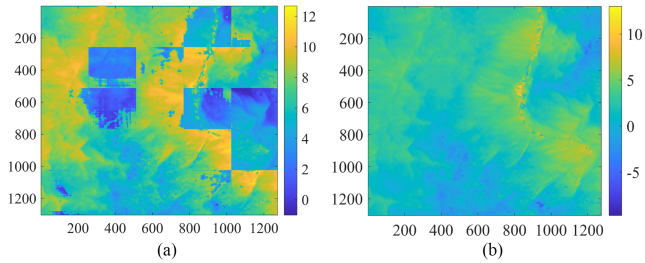

Fig. 12. FPUNet one-step and two-step phase unwrapping results. (a) One-step. (b) Two-step.

of phase unwrapping obtained by the two networks. The results are shown in Table VIII, and it is evident from the data in the table that the average absolute error and root-mean-square error of one-step phase unwrapping of FPUNet are more significant than the error values of two-step phase unwrapping, which are 4.048 and 4.852 rad, respectively. This finding emphasizes that the two-step unwrapping approach may be more effective for a given task. In addition, looking further at Fig. 12, we find that one-step phase deconvolution has many discontinuous regions after deconvolution splicing in the actual data region. Such discontinuities may lead to instability in the unwrapping results, especially in complex scenarios. Two-step unwrapping can adjust the phase more carefully, which can better handle these discontinuities and produce more continuous and accurate unwrapping results. Therefore, although one-step unwrapping has theoretical end-to-end advantages, the selective use of unwrapping methods for specific scenarios is crucial in practical applications.

F. Uniqueness of the FPUNet Phase Unwrapping Algorithm

In the field of InSAR, the accuracy of phase unwrapping is crucial for the accuracy of elevation or deformation rate, especially in complex mountainous areas and high-noise regions with large gradient changes. In the past, most phase unwrapping algorithms based on deep learning have been experimented with using simulation data. At the same time, the research in this article focuses more on verifying the reliability of the algorithms using actual data. In this study, the FPUNet phase unwrapping algorithm is proposed, and its core idea is to use deep learning networks to solve the phase unwrapping problem quickly. It is worth noting that we have not neglected the importance of the SDPC algorithm when parsing the FPUNet phase unwrapping algorithm. The SDPC algorithm provides a critical preprocessing step for FPUNet. In the region of high noise and large

gradient variations, the SDPC algorithm can robustly provide accurate phase unwrapping results, which provides a reliable basis for the input data of FPUNet. Therefore, in this article, the SDPC algorithm is regarded as an essential part of the FPUNet phase unwrapping algorithm, and the two complement each other to improve the accuracy and efficiency of phase unwrapping. By combining FPUNet with the SDPC algorithm, this study aims to provide a novel approach to solving the phase unwrapping problem in InSAR, demonstrating excellent robustness and accuracy in practical applications.

Currently, some phase unwrapping algorithms based on deep learning utilize existing digital elevation models (DEMs), such as SRTM DEM, as references for phase unwrapping. However, this approach differs from the method described in this article. InSAR technology aims to unwrap interferometric phases to obtain phase information of target objects and elevation information is then derived through a series of inversion methods. We recognize that DEMs are not equivalent to phase unwrapping, and DEMs such as SRTM DEM are not updated in real time. Consequently, changes in terrain may occur in some areas due to factors such as natural disasters or human activities, meaning that SRTM DEM may not capture these changes. In deep learning, using DEMs as references for phase unwrapping may be an approximate approach. In contrast, our method, utilizing phase unwrapping results obtained from the SDPC algorithm based on real-time interferometric phases as the output layer of deep learning, can achieve results closer to actual phase unwrapping results with higher accuracy.

G. Comparative Analysis of Existing Deep Learning Phase Unwrapping Models: A Necessity?

In this article, we introduce a method called the sliding window singular value correction model phase gradient corrected unwrapping (SDPC) algorithm, aimed at addressing the challenge of practical phase unwrapping in complex mountainous areas with high noise and large gradient regions. Unlike previous literature, our focus is not on comparing the performance of deep learning phase unwrapping models but on highlighting the advantages of the SDPC method in addressing phase unwrapping in high noise and large gradient regions. The SDPC algorithm, by introducing a sliding window singular value corrected model, can effectively perform phase unwrapping in areas with high noise and large gradient changes. We conducted a series of experiments to validate the superiority and accuracy of SDPC over traditional InSAR phase unwrapping methods (such as the branch cutting method, the ILS method, and the MCF method). The results demonstrate that SDPC performs remarkably well in these challenging scenarios.

However, the SDPC method faces challenges in terms of processing efficiency because it requires iterative computations. To address this challenge, we have introduced deep learning technology. Integrating deep learning techniques can accelerate the unwrapping process and achieve rapid InSAR phase unwrapping. Unlike research papers solely relying on deep learning for phase unwrapping, the field of deep learning phase unwrapping has witnessed the emergence of numerous new models, such as PGNet, BCNet, and PUGAN [37], [38], [39]. Depending on the learning objectives, deep learning-based phase unwrapping methods include one-step phase unwrapping, two-step phase unwrapping, phase gradient estimation methods, and BC deployment methods. PGNet, BCNet, and PUGAN belong to phase gradient estimation, BC deployment, and one-step phase unwrapping methods, respectively. In contrast, the FPUNet used in this article belongs to the two-step phase unwrapping method. Each of these methods has its advantages. Of course, for both phase unwrapping and two-step phase unwrapping methods, if the performance of the deep learning network model itself is good, then using the same dataset will undoubtedly yield better results. Therefore, we did not compare it with other deep learning models for the reasons above.

H. Shortcomings of the Proposed Method in This Article

Through a series of experiments and comparisons, the proposed method in this article has been effectively demonstrated to quickly and efficiently obtain InSAR phase unwrapping results in regions of high noise and large gradient variations. However, the proposed method still needs some improvement. 1) When using the SDPC algorithm for phase unwrapping, a single interferometric phase point needs to be selected, and phase unwrapping is performed using the ILS method. Experimentally, however, it has been found that different choices of the interferometric phase points can lead to different degrees of discrepancy in the results. Therefore, efficiently and accurately selecting an interferometric phase point has become an essential technical difficulty in investigating and addressing in future studies. 2) When building the FPUNet network sample set, the empirical sample set selected A region as the sample set for learning and training. However, this choice may lead to sample features that do not generalize well. In the future, we will focus on exploring whether randomly selecting data of size 256×256 pixels from the entire region as the sample set can effectively improve the phase unwrapping accuracy of FPUNet. 3) The FPUNet network proposed in this article is an enhanced network model derived from ResUNet by incorporating a convolutional block attention module. This module aims to enhance the accuracy of different network models, given the remarkable advancements of the Transformer model in natural language processing, computer vision, and other domains, including the transformative ChatGPT technology. It is worth exploring whether introducing Transformer into the network model of this article can further accelerate processing efficiency and accuracy.

VII. Conclusion

In complex mountainous regions, achieving precise and efficient phase unwrapping results is challenging due to high noise and regions with significant gradient variations. This article introduces a rapid InSAR phase unwrapping approach for regions characterized by high noise and large gradient variations in complex mountainous areas. The study focuses on the Dongchuan District of Kunming City in Yunnan Province, China. Simulated data were introduced since the measured interferometric phase

data could not determine the true phase. Through a series of experimental results, the following conclusions were reached.

1) In the simulation experiments with high noise level data, the SDPC phase unwrapping algorithm demonstrated superior performance in unwrapping the phase in areas with significant gradient changes, yielding results that closely align with the true phase. Consequently, it exhibits enhanced accuracy and overall performance compared to other phase unwrapping algorithms.
2) In the validation experiments with measured interferometric phase data, the SDPC algorithm performed excellently under natural noise conditions, surpassing the other three phase unwrapping algorithms regarding mean absolute and root-mean-square errors. Moreover, the phase unwrapping results obtained by the SDPC algorithm exhibited consistency with the true curve and displayed minimal jump bias compared to the other algorithms.
3) The postprocessing method proposed in this study effectively reduces the portion of the phase that cannot be accurately predicted by the deep learning model, thereby enhancing the quality of the phase unwrapping results. In validation sets C and D, the phase unwrapping results achieved by FPUNet align well with those obtained by the SDPC algorithm. Notably, in region D, the similarity curve generated by the FPUNet unwrapping algorithm exhibits smoother characteristics compared to the SDPC algorithm.
4) For region D, the fastest time for ILS is 2.5 s, but ILS does not effectively guarantee the quality of the unwrapping, while the time required for unwrapping with FPUNet is 8.975 s. Although its time is not the fastest compared to ILS, it demonstrates powerful performance, can guarantee unwrapping accuracy, and takes into account the processing efficiency in regions with high noise and larger gradient variations.
5) The FPUNet phase unwrapping algorithm has a substantial transfer and generalization capability. That is, it does not require the acquisition of unwrapped phase information corresponding to different interference phases at different periods to construct the training sample set of the FPUNet network, which effectively improves its efficiency and adaptability in practical applications.

In summary, the proposed SDPC algorithm demonstrates excellent performance in the face of complex mountainous regions with high noise and large gradient variations and can obtain accurate unwrapping results. Meanwhile, combining the FPUNet algorithm can further improve the unwrapping efficiency and processing speed. These results provide valuable references and demonstrate applications to the phase unwrapping problem in complex mountainous regions.

ACKNOWLEDGMENT

The authors would like to thank the anonymous reviewers for their valuable feedback on the manuscript. The authors also would like to thank ESA for providing the Sentinel 1 data.

REFERENCES

[1] E. Chaussard, S. Wdowinski, E. Cabral-Cano, and F. Amelung, "Land subsidence in central Mexico detected by ALOS InSAR time-series," *Remote Sens. Environ.*, vol. 140, pp. 94–106, Jan. 2014.
[2] F. Cigna and D. Tapete, "Satellite InSAR survey of structurally-controlled land subsidence due to groundwater exploitation in the Aguascalientes Valley, Mexico," *Remote Sens. Environ.*, vol. 254, Mar. 2021, Art. no. 112254.
[3] B. Osmanoğlu, F. Sunar, S. Wdowinski, and E. Cabral-Cano, "Time series analysis of InSAR data: Methods and trends," *ISPRS J. Photogrammetry Remote Sens.*, vol. 115, pp. 90–102, May 2016.
[4] M. Costantini, "A novel phase unwrapping method based on network programming," *IEEE Trans. Geosci. Remote Sens.*, vol. 36, no. 3, pp. 813–821, May 1998.
[5] Z.-F. Ma, M. Jiang, M. Khoshmanesh, and X. Cheng, "Time series phase unwrapping based on graph theory and compressed sensing," *IEEE Trans. Geosci. Remote Sens.*, vol. 60, 2022, Art. no. 5204412.
[6] H. Yu, Y. Lan, Z. Yuan, J. Xu, and H. Lee, "Phase unwrapping in InSAR: A review," *IEEE Geosci. Remote Sens. Mag.*, vol. 7, no. 1, pp. 40–58, Mar. 2019.
[7] F. Sica, F. Calvanese, G. Scarpa, and P. Rizzoli, "A CNN-based coherence-driven approach for InSAR phase unwrapping," *IEEE Geosci. Remote Sens. Lett.*, vol. 19, 2022, Art. no. 4003705.
[8] R. M. Goldstein, H. A. Zebker, and C. L. Werner, "Satellite radar interferometry: Two-dimensional phase unwrapping," *Radio Sci.*, vol. 23, pp. 713–720, Aug. 1988.
[9] R. R. Garcia and A. Zakhor, "Consistent stereo-assisted absolute phase unwrapping methods for structured light systems," *IEEE J. Sel. Topics Signal Process.*, vol. 6, no. 5, pp. 411–424, Sep. 2012.
[10] D. L. Fried, "Least-square fitting a wave-front distortion estimate to an array of phase-difference measurements," *J. Opt. Soc. Am.*, vol. 67, pp. 370–375, Mar. 1977.
[11] D. C. Ghiglia and L. A. Romero, "Minimum L(p)-norm two-dimensional phase unwrapping," *J. Opt. Soc. Amer. A-Opt. Image Sci. Vis.*, vol. 13, pp. 1999–2013, Oct. 1996.
[12] C. Chen and H. Zebker, "Two-dimensional phase unwrapping with use of statistical models for cost functions in nonlinear optimization," *J. Opt. Soc. Amer. A-Opt. Image Sci. Vis.*, vol. 18, pp. 338–351, Feb. 2001.
[13] A. Pepe and R. Lanari, "On the extension of the minimum cost flow algorithm for phase unwrapping of multitemporal differential SAR interferograms," *IEEE Trans. Geosci. Remote Sens.*, vol. 44, no. 9, pp. 2374–2383, Aug. 2006.
[14] O. Loffeld, H. Nies, S. Knedlik, and W. Yu, "Phase unwrapping for SAR interferometry—A data fusion approach by Kalman filtering," *IEEE Trans. Geosci. Remote Sens.*, vol. 46, no. 1, pp. 47–58, Jan. 2008.
[15] V. Pascazio and G. Schirinzi, "Estimation of terrain elevation by multifrequency interferometric wide band SAR data," *IEEE Signal Process. Lett.*, vol. 8, no. 1, pp. 7–9, Jan. 2001.
[16] H. Yu and Y. Lan, "Robust two-dimensional phase unwrapping for multi-baseline SAR interferograms: A two-stage programming approach," *IEEE Trans. Geosci. Remote Sens.*, vol. 54, no. 9, pp. 5217–5225, Sep. 2016.
[17] Y. Guo, X. Chen, and T. Zhang, "Robust phase unwrapping algorithm based on least squares," *Opt. Lasers Eng.*, vol. 63, pp. 25–29, Dec. 2014.
[18] L. Yan, H. Zhang, R. Zhang, X. Xie, and B. Chen, "A robust phase unwrapping algorithm based on reliability mask and weighted minimum least-squares method," *Opt. Lasers Eng.*, vol. 112, pp. 39–45, Jan. 2019.
[19] J. Kang, D. Hong, J. Liu, G. Baier, N. Yokoya, and B. Demir, "Learning convolutional sparse coding on complex domain for interferometric phase restoration," *IEEE Trans. Neural Netw. Learn. Syst.*, vol. 32, no. 2, pp. 826–840, Feb. 2021.
[20] J. Qian et al., "Deep-learning-enabled geometric constraints and phase unwrapping for single-shot absolute 3D shape measurement," *APL Photonics*, vol. 5, Apr. 2020, Art. no. 046105.
[21] G. E. Spoorthi, S. Gorthi, and R. K. S. S. Gorthi, "PhaseNet: A deep convolutional neural network for two-dimensional phase unwrapping," *IEEE Signal Process. Lett.*, vol. 26, no. 1, pp. 54–58, Jan. 2019.
[22] K. Wang, Y. Li, Q. Kemao, J. Di, and J. Zhao, "One-step robust deep learning phase unwrapping," *Opt. Exp.*, vol. 27, pp. 15100–15115, May 2019.
[23] H. T. Xia, Z. B. Fan, H. M. Cheng, and B. C. Yang, "Non-invasive mechanical measurement for transparent objects by digital holographic interferometry based on iterative least-squares phase unwrapping," *Exp. Mech.*, vol. 52, pp. 439–445, Jun. 2011.
[24] H. Xia et al., "Phase calibration unwrapping algorithm for phase data corrupted by strong decorrelation speckle noise," *Opt. Exp.*, vol. 24, pp. 28713–28730, Dec. 2016.

[25] M. D. Pritt, "Phase unwrapping by means of multigrid techniques for interferometric SAR," *IEEE Trans. Geosci. Remote Sens.*, vol. 34, no. 3, pp. 728–738, May 1996.
[26] N. Ibtehaz and M. S. Rahman, "MultiResUNet : Rethinking the U-net architecture for multimodal biomedical image segmentation," *Neural Netw.*, vol. 121, pp. 74–87, Jan. 2020.
[27] D. John and C. Zhang, "An attention-based U-net for detecting deforestation within satellite sensor imagery," *Int. J. Appl. Earth Observ. Geoinf.*, vol. 107, Mar. 2022, Art. no. 102685.
[28] X. He, Y. Zhou, J. Zhao, D. Zhang, R. Yao, and Y. Xue, "Swin transformer embedding UNet for remote sensing image semantic segmentation," *IEEE Trans. Geosci. Remote Sens.*, vol. 60, 2022, Art. no. 4408715.
[29] Z. Zhang, Q. Liu, and Y. Wang, "Road extraction by deep residual U-net," *IEEE Geosci. Remote Sens. Lett.*, vol. 15, no. 5, pp. 749–753, May 2018.
[30] K. He, X. Zhang, S. Ren, and J. Sun, "Deep residual learning for image recognition," in *Proc. IEEE Conf. Comput. Vis. Pattern Recognit.*, Jun. 2016, pp. 770–778.
[31] S. Woo, J. Park, J. Y. Lee, and I. S. Kweon, "CBAM: Convolutional block attention module," in *Proc. Eur. Conf. Comput. Vis.*, 2018, vol. 11211, pp. 3–19.
[32] O. Ronneberger, P. Fischer, and T. Brox, "U-Net: Convolutional networks for biomedical image segmentation," in *Proc. Int. Conf. Med. Image Comput. Comput.-Assist. Intervent.*, 2015, vol. 9351, pp. 234–241.
[33] S. Ioffe and C. Szegedy, "Batch normalization: Accelerating deep network training by reducing internal covariate shift," in *Proc. Int. Conf. Mach. Learn.*, Jul. 2015, pp. 448–456.
[34] L. Zhou, H. Yu, and Y. Lan, "Deep convolutional neural network-based robust phase gradient estimation for two-dimensional phase unwrapping using SAR interferograms," *IEEE Trans. Geosci. Remote Sens.*, vol. 58, no. 7, pp. 4653–4665, Jul. 2020.
[35] W. Yin et al., "Temporal phase unwrapping using deep learning," *Sci. Rep.*, vol. 9, Dec. 2019, Art. no. 20175.
[36] D. P. Kingma and J. Ba, "Adam: A method for stochastic optimization," 2014, *arXiv:1412.6980*.
[37] L. Zhou, H Yu, and Y Lan, "Deep convolutional neural network-based robust phase gradient estimation for two-dimensional phase unwrapping using SAR interferograms," *IEEE Trans. Geosci. Remote Sens.*, vol. 58, no. 7, pp. 4653–4665, Jul. 2020.
[38] L. Zhou, H. Yu, Y. Lan, and M. Xing, "Deep learning-based branch-cut method for InSAR two-dimensional phase unwrapping," *IEEE Trans. Geosci. Remote Sens.*, vol. 60, 2022, Art. no. 5209615.
[39] L. Zhou, H. Yu, V. Pascazio, and M. Xing, "PU-GAN: A one-step 2-D InSAR phase unwrapping based on conditional generative adversarial network," *IEEE Trans. Geosci. Remote Sens.*, vol. 60, 2022, Art. no. 5221510.

Dingyi Zhou received the B.S. degree in surveying and mapping engineering from Yunnan Normal University, Kunming, China, in 2018, and the M.S. degree in cartography and Geographic information systems from Kunming University of Science and Technology, Kunming, in 2022. He is currently working toward the Ph.D. degree in cartography and geographic information systems with Yunnan University, Kunming.

His main research interests include the principle and application of the synthetic aperture radar interferometry (InSAR) algorithm.

Zhifang Zhao received the B.S. degree in geomorphology and quaternary geology from Nanjing University, Nanjing, China, in 1992, and the Ph.D. degree in geological resources and geological engineering, specializing in resource and environment remote sensing, from China University of Geosciences, Beijing, China, in 2009.

She has been serving as a Professor with the Department of Earth Sciences, Yunnan University, Kunming, China, since 2009. Her research interests include utilizing synthetic aperture radar interferometry (InSAR) to monitor geological phenomena deformation and conduct deformation genesis analysis.